J Solid State Electrochem (2011) 15:1243–1251
DOI 10.1007/s10008-010-1194-6

ORIGINAL PAPER

Effect of mono- (Cr) and bication (Cr, V) substitution on $LiMn_2O_4$ spinel cathodes

N. Jayaprakash · N. Kalaiselvi · Gangulibabu · D. Bhuvaneswari

Received: 10 February 2010 / Revised: 2 September 2010 / Accepted: 6 September 2010 / Published online: 19 September 2010

Abstract A study on the structural and electrochemical properties of $LiCr_{0.2}Mn_{1.8}O_4$ and $LiV_{0.2}Cr_{0.2}Mn_{1.6}O_4$ cathodes has been made with a view to understand the effect of mono- (Cr) and bication (Cr and V) substitution on $LiMn_2O_4$ spinel individually. Citric acid assisted modified sol–gel method has been followed to synthesize a series of $LiMn_2O_4$, $LiCr_{0.2}Mn_{1.8}O_4$, and $LiV_{0.2}Cr_{0.2}Mn_{1.6}O_4$ cathodes, and the corresponding lattice structure, surface morphology, and site occupancy of lithium in the spinel matrix are acknowledged using X-ray diffraction, scanning electron microscopy, and magic angle spinning ^{7}Li nuclear magnetic resonance results. The site occupancy of Cr^{3+} in the *16d* octahedral and that of V^{5+} in the *16d* octahedral and *8a* tetrahedral positions are understood. Electrochemical cycling studies of $LiCr_{0.2}Mn_{1.8}O_4$ cathode demonstrate an enhanced structural stability and better capacity retention (94%) resulting from the Cr^{3+} dopant-induced co-valency of Li-O-Mn bond. On the other hand, simultaneous substitution of Cr and V in $LiV_{0.2}Cr_{0.2}Mn_{1.6}O_4$ has failed to improve the electrochemical properties of native $LiMn_2O_4$ spinel cathode, mainly due to vanadium-driven cation mixing and the reduced lithium diffusion kinetics. Among the candidates chosen for the study, $LiCr_{0.2}Mn_{1.8}O_4$ qualifies itself as a better cathode for rechargeable lithium battery applications.

Keywords $LiMn_2O_4$ cathodes · Cr and V doping · MAS ^{7}Li-NMR · Lithium-ion batteries

N. Jayaprakash · N. Kalaiselvi (✉) · Gangulibabu · D. Bhuvaneswari
Central Electrochemical Research Institute, Karaikudi, India 630 006
e-mail: kalakanth2@yahoo.com

Introduction

Spinel $LiMn_2O_4$ has long been exploited as a possible cathode material for lithium-ion battery applications [1]. Besides being eco-benign in nature, the easy-to-adopt synthesis condition and the economical viability of $LiMn_2O_4$ cathode make it a suitable alternate to the commercially upgraded $LiCoO_2$ cathode [2]. The $LiMn_2O_4$ cathode material has a cubic spinel structure, in which the lithium ions occupy *8a* tetrahedral interstices and the manganese cations occupy *16d* octahedral interstices of a cubic close-packed array constituted by the oxygen atoms located in the *32e* positions of the *Fd3m* space group [3]. Herein, lithium ions exhibit a relatively rapid diffusion through a pathway consisting of *8a* and *16c* sites. Despite the fact that $LiMn_2O_4$ spinel represents a cheap and an alternative cathode for $LiCoO_2$, not more than 100–110 mAh/g has been achieved practically against the theoretical capacity of 148 mAh/g [4]. In addition, the unacceptable capacity fade of spinels has prompted renewed research interest on $LiMn_2O_4$ cathode to identify, to understand and to address the same [5-7]. Towards this direction, surface-treated spinels and lithium excess spinels are considered as remedial measures to alleviate the capacity fade issue apart from the adoption of suitably selected synthesis method and the formation of solid solutions by partially replacing Mn^{3+}ions.

Among the various metals that can partially replace Mn^{3+} ions, Cr^{3+}, similar in size to Mn^{3+}, is reported to form the robust spinel structure [8, 9] via Cr^{3+}-driven increased co-valency of Li-O-Mn bond [10]. In addition, Cr^{3+} substitution facilitates the presence of lithium that is pinned in the T_d site near the octahedral Mn ions and hence prevents the formation of a series of cation-ordered phases during charging [4]. However, a capacity decrease

in the voltage range of 3.5–4.3 V is reported for Cr^{3+} substitution, which holds good for higher Cr^{3+} concentration. Because Sigala et al. [11] have reported satisfactory cycleability for $x \leq 0.5$ and lower capacity loss at $x_1=0.25$ for Cr^{3+}-substituted $LiMn_2O_4$ spinels, Cr^{3+} has been chosen as a metal dopant, and the concentration of the same has been fixed as 10% ($x_1=0.20$) for the present study.

Considering the bication substitution in $LiMn_2O_4$, based on the simple fact that high-valence (>+4) metal ions are attractive [12] in suppressing the structural transformation during charge–discharge process, pentavalent vanadium has been chosen as the other dopant. Since it is well-known that the valency of manganese ions become almost +3 for a higher concentration of vanadium ($x \geq 0.4$), as the substitution of Mn with V^{5+} forces Mn^{4+} to reduce to Mn^{3+} by valence compensation, a nominal concentration of 10% ($x_2=0.20$) has been chosen for vanadium dopant.

The present communication is focused on the understanding of individual effect of mono- (Cr^{3+}) and bication (Cr^{3+} and V^{5+}) substituted on $LiMn_2O_4$ cathode in addressing the hampering issues that are concerned with the unacceptable capacity fade and the poor cycle life behavior of spinel cathode. Particularly, this is the first ever attempt made to explore the electrochemical characteristics of pentavalent V dopant in association with the Cr^{3+} dopant in $LiMn_2O_4$ spinel cathode, and the same is the significance of the study.

A set of spinel cathodes containing undoped $LiMn_2O_4$, monocation-doped $LiCr_{0.2}Mn_{1.8}O_4$, and bication-doped $LiV_{0.2}Cr_{0.2}Mn_{1.6}O_4$ compounds were synthesized by following citric acid assisted modified sol–gel (CAM sol–gel) method [13] and characterized individually for their physical as well as electrochemical performance.

Experimental

Synthesis procedure

The $LiMn_2O_4$-based active materials planned for the study were synthesized by adopting CAM sol–gel method, wherein the reaction proceeds in an acidic environment created by the addition of an organic acid. Stoichiometric proportions of high-purity reactants, viz., CH_3COOLi, $Mn(CH_3COO)_2.4H_2O$, $Cr(NO_3)_3.9H_2O$ (for doping Cr), and NH_4VO_3 (for doping V) (Sigma Aldrich, India) were selected as precursors and citric acid was added as a complexing agent, followed by the addition of acryl amide and N,N′-methylene bis acryl amide. Details pertaining to the CAM sol–gel synthesis approach, role of various additives deployed in the synthesis methodology, and the precautionary measures to be adhered during the process of furnace calcination are discussed elsewhere [14].

Physical and electrochemical characterization

Phase characterization was done from the powder X-ray diffraction (XRD) patterns recorded on a Philips 1830 X-ray diffractometer using Ni-filtered Cu-Kα radiation (λ= 1.5406 Å) in the 2θ range of 10–80° at a scan rate of 0.04° s^{-1}. Surface morphology and the percentage composition of various elements/metals present in the synthesized active materials were investigated using scanning electron microscopy (SEM) coupled with energy-dispersive X-ray analysis (EDAX) results obtained from Jeol S-3000 H scanning electron microscope. Chemical compositions of prepared compounds were verified from atomic absorption spectrophotometer (VARIAN model) SpectrAA 220. ^{7}Li nuclear magnetic resonance (NMR) measurements were carried out with a Bruker MSL-400 spectrometer by employing a 5-mm Bruker variable-temperature magic-angle spinning (MAS) probe operating at a ^{7}Li frequency of 14 MHz. For the current study, a one-pulse sequence was used with a pulse length of 3 μs along with a recycle delay of 500 ms for about 100,000 scans. Room-temperature electrochemical studies such as cyclic voltammetry (CV) and charge–discharge measurements were performed using an Autolab Electrochemical Workstation and MACCOR charge–discharge cycle life tester. In this connection, both the electrochemical characterization were performed with crimp-sealed 2016 coin cells containing lithium metal anode synthesized $LiMn_2O_4$-based cathode and a non-aqueous electrolyte containing 1 M $LiPF_6$ salt dissolved in 1:1 *v*/*v* ethylene carbonate and dimethyl carbonate solvent.

Electrode preparation and cell assembly

The process of electrode preparation and the coin cell fabrication in an argon-filled glove box are mentioned in our earlier reports [15].

Results and discussion

Structural results—PXRD studies

Figure 1 shows the powder XRD (PXRD) patterns observed for the synthesized compounds, viz., $LiMn_2O_4$, $LiCr_{0.2}Mn_{1.8}O_4$, and $LiV_{0.2}Cr_{0.2}Mn_{1.6}O_4$. Existence of sharp and well-defined Bragg peaks with no extra peaks illuminates the formation of highly crystalline and phase-pure products. The miller indices (*hkl*) of all the peaks corresponding to the unsubstituted $LiMn_2O_4$ and its doped derivatives were indexed to a cubic crystal lattice structure with *Fd3m* space group, based on the Joint Committee on Powder Diffraction Standards (JCPDS) pattern (file no: 35-

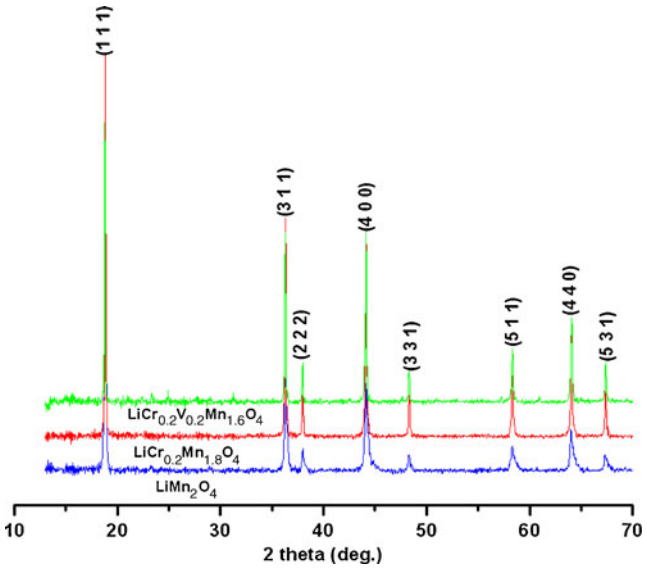

Fig. 1 XRD pattern of $LiM_{1x}M_{2y}Mn_{2-x-y}O_4$ (M_1=Cr, M_2=V; x=y=0.2) cathodes

0782). The lattice parameter value calculated from the assigned miller indices is a=8.145 ($LiMn_2O_4$), 8.147 ($LiCr_{0.2}Mn_{1.8}O_4$), and 8.176 Å ($LiV_{0.2}Cr_{0.2}Mn_{1.6}O_4$).

In $LiCr_{0.2}Mn_{1.8}O_4$ compound, the trivalent Cr (0.615 Å) is expected to replace the Mn^{3+} ions (0.645 Å) and to increase the average oxidation state of Mn beyond 3.5. On the other hand, the calculated lattice parameter value (a= 8.147) coincides with the reported values of $LiMn_2O_4$ containing slightly excess concentration of lithium (JCPDS nos. 89-460 and 89-0753). This may be considered as an indication that the average oxidation state of Mn is not increased to a desirable extent due to the incorporation of Cr^{3+} dopant, and hence it is believed at this point that Cr^{3+} substitution would be less effective in improving the electrochemical behavior of native $LiMn_2O_4$ compound. However, since the octahedral stabilization energy of Cr^{3+} (224.83 KJ/mol) is more than that of Mn^{3+} (135.65 KJ/mol) [16], partial substitution of Mn^{3+} with Cr^{3+} is expected to stabilize the native $LiMn_2O_4$ structure with the select concentration of x_1=0.20.

On the other hand, the calculated lattice parameter value of $LiV_{0.2}Cr_{0.2}Mn_{1.6}O_4$ compound (a=8.176 Å) corresponds to that of $LiMn_2O_4$ containing slightly lesser concentration of lithium (JCPDS no. 88-1608). Such a reduced concentration of lithium results from the charge compensation of V^{5+} substituted for Mn^{4+}, and hence the average oxidation state of Mn in $LiV_{0.2}Cr_{0.2}Mn_{1.6}O_4$ compound would fall below 3.5, which is the Jahn–Teller distortion region. The same is better understood from the larger difference in 'a' value (8.176 Å) calculated for $LiV_{0.2}Cr_{0.2}Mn_{1.6}O_4$, compared to the parent $LiMn_2O_4$ (8.145 Å). Unlike the literature report [12] that a higher concentration of vanadium (x=0.30) would lead to a random occupation in both T_d and O_h sites, the currently deployed 10% vanadium itself is believed to reduce the vacancies in the T_d and O_h sites of $LiMn_2O_4$ spinel, which may impart an adverse effect upon electrochemical behavior.

Morphological results—SEM analysis

Scanning electron micrographs of $LiMn_2O_4$, $LiCr_{0.2}Mn_{1.8}O_4$, and $LiV_{0.2}Cr_{0.2}Mn_{1.6}O_4$ powders prepared at 800 °C are shown in Fig. 2a–c. The existence of finer particle surface with well-defined grain boundaries is obvious from the SEM images. Unlike the parent $LiMn_2O_4$ (Fig. 2a), no particle agglomeration is observed for the doped derivatives, wherein the compounds (Fig. 2b, c) exhibited a spherical morphology formed by the combination of a large number of size-reduced particles.

Further, the stoichiometry of the synthesized cathode materials was investigated using EDAX analysis (Fig. 3a–c), wherein the percentage of the individual elements has been confirmed with an exception of Li, as it is not possible to calculate the percentage of lithium using EDAX. However, the concentration of lithium has been verified from AAS studies, which is in accordance with the results derived from XRD analysis.

^{7}Li MAS-NMR spectral studies

The ^{7}Li MAS-NMR spectra of $LiMn_2O_4$, $LiCr_{0.2}Mn_{1.8}O_4$ and $LiV_{0.2}Cr_{0.2}Mn_{1.6}O_4$ synthesized at 800 °C are depicted in Fig. 4a–c. Presence of two intense resonances around 525 and 620 ppm is seen for $LiMn_2O_4$ and $LiCr_{0.2}Mn_{1.8}O_4$, whereas an additional resonance at 0 ppm is observed for $LiMn_{1.6}Cr_{0.2}V_{0.2}O_4$ sample.

The major resonance at ~525 ppm of $LiMn_2O_4$ (Fig. 4a) is assigned to a lithium cation in the normal tetrahedral *8a* site of the spinel structure [17], and the second intense resonance at 620 ppm may be assigned to lithium cations surrounding the defects, consisting of *16d* manganese vacancies [18]. Further, the close resemblance in the ^{7}Li NMR pattern of $LiCr_{0.2}Mn_{1.8}O_4$ (Fig. 4b) with the parent $LiMn_2O_4$ corresponds to the fact that the partial substitution of Cr^{3+} (for Mn^{3+}) has taken place in the *16d* site without affecting the lithium local environment significantly.

On the other hand, the existence of a new peak at 0 ppm in ^{7}Li NMR spectrum of $LiV_{0.2}Cr_{0.2}Mn_{1.6}O_4$ compound (Fig. 4c) indicates the possible and partial occupation of V^{5+} ions in the 8a tetrahedral interstices, which in turn may lead to the occupation of fraction of lithium ions in an additional site also. Generally, such a situation may result from the unavoidable presence of some pentavalent vanadium (dopant)-based impurity also. However, unlike the previous study on $LiV_{0.2}Cr_{0.2}Mn_{1.6}O_{3.8}F_{0.2}$ compound [19], presence of undesirable Li-V-O impurity is not

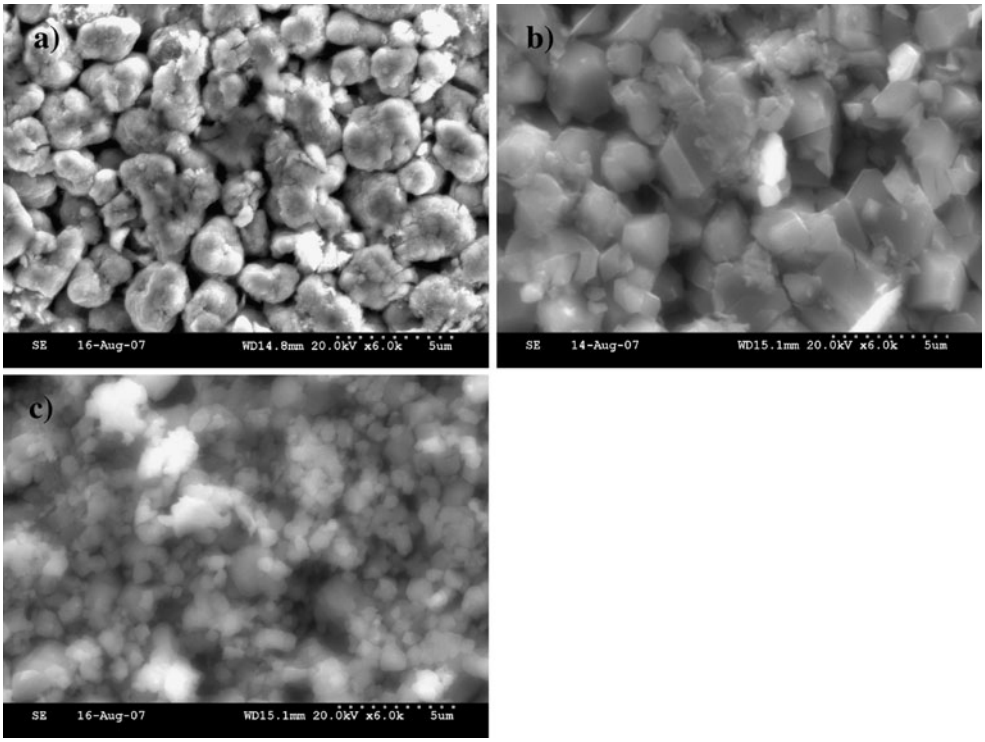

Fig. 2 SEM images of **a** $LiMn_2O_4$, **b** $LiCr_{0.2}Mn_{1.8}O_4$, and **c** $LiV_{0.2}Cr_{0.2}Mn_{1.6}O_4$

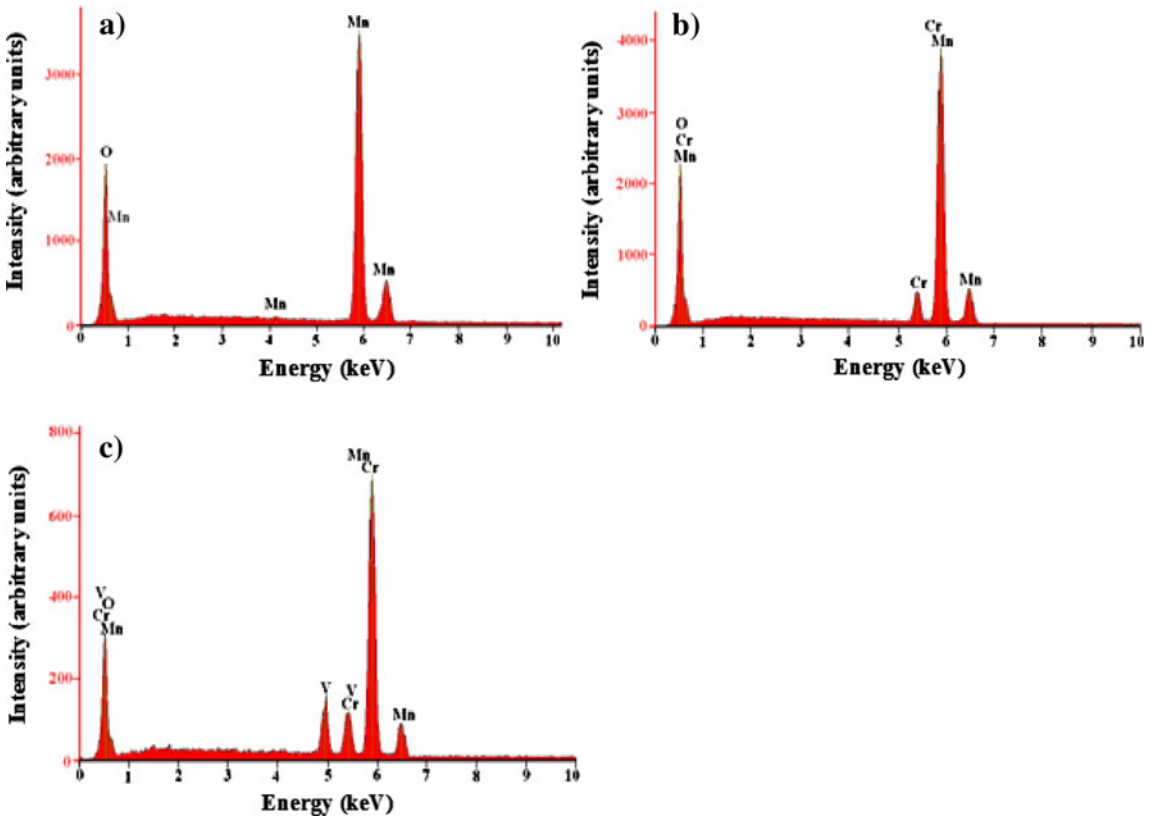

Fig. 3 EDAX analysis of **a** $LiMn_2O_4$, **b** $LiCr_{0.2}Mn_{1.8}O_4$, and **c** $LiV_{0.2}Cr_{0.2}Mn_{1.6}O_4$

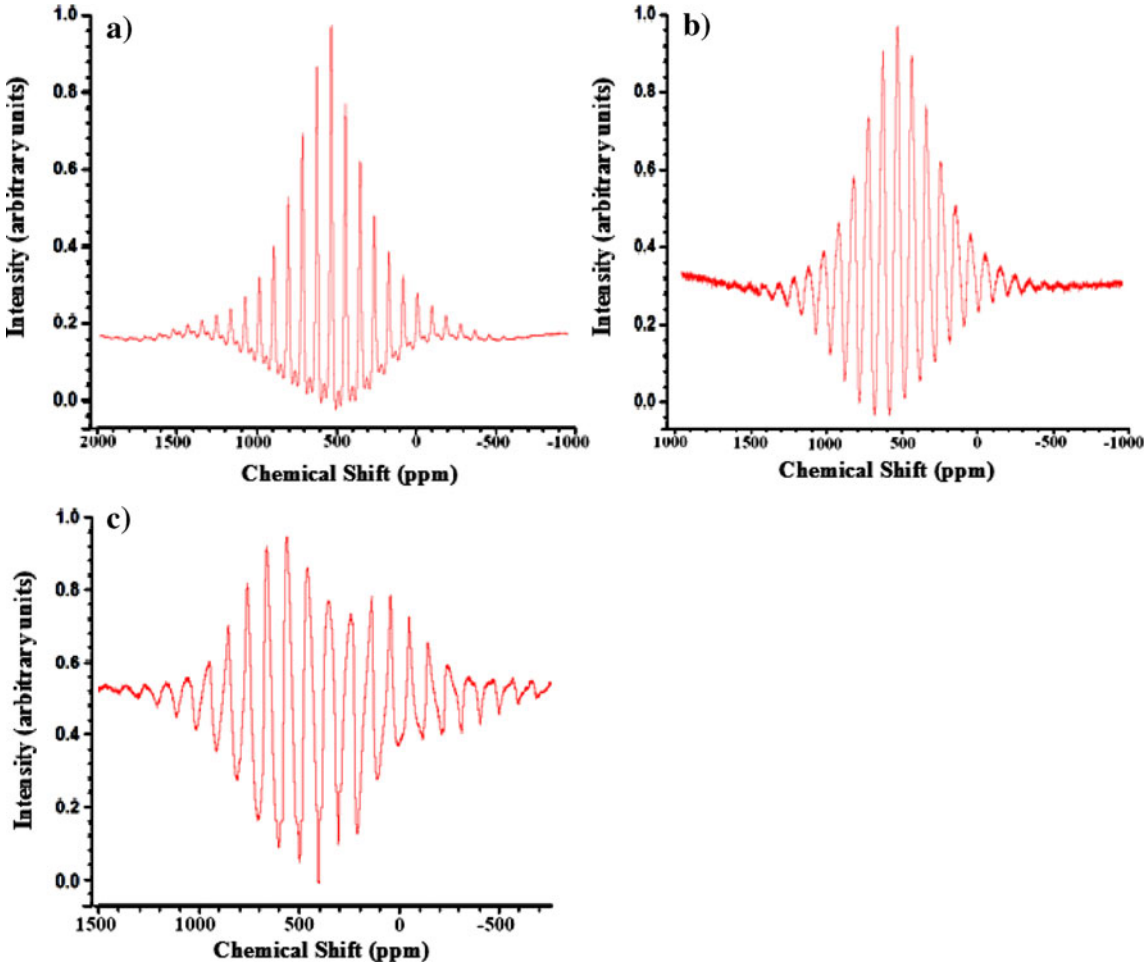

Fig. 4 ^{7}Li NMR spectra of **a** $LiMn_2O_4$, **b** $LiCr_{0.2}Mn_{1.8}O_4$, and **c** $LiV_{0.2}Cr_{0.2}Mn_{1.6}O_4$

evident from the PXRD pattern of $LiV_{0.2}Cr_{0.2}Mn_{1.6}O_4$. Therefore, the presence of an additional resonance at 0 ppm may be attributed to the combined effect of *8a* tetrahedral site-occupied vanadium dopant and the Jahn–Teller distorted manganese-induced defect mechanism that drives some of the Li^+ ions to occupy sites other than *8a* and the near *16d* manganese vacant sites, which is ambiguous. A detailed investigation pertaining to the role of V^{5+} dopant with and without the presence of Cr^{3+} dopant in a variety of other lithium intercalating matrices such as $LiMPO_4$ and $LiMSiO_4$ would offer more information and understanding on this issue. However, the presence of an additional resonance at 0 ppm observed with the $LiV_{0.2}Cr_{0.2}Mn_{1.6}O_4$ compound could be correlated to the existence of solid solution consisting of bication-substituted $LiMn_2O_4$ based on the aforesaid factors of V^{5+}-driven cation mixing, despite the fact that the presence of a single and an intense peak at 0 ppm is the characteristic behavior of a fully diamagnetic compound [19].

Electrochemical characterization

Cyclic voltammetry studies

CV study was performed on $Li/LiMn_2O_4$, $Li/LiCr_{0.2}Mn_{1.8}O_4$, and $Li/LiV_{0.2}Cr_{0.2}Mn_{1.6}O_4$ half cells with an aim to investigate upon the effect of dopants over the diffusion kinetics of lithium [20]. Figure 5a–c shows the cyclic voltammograms of the synthesized compounds recorded at room temperature under a scan rate of 0.5 mV/s between a wide potential range of 2.0 to 4.5 V with a view to understand the effect of dopants upon progressive cycling.

The CV pattern of all the cathodes shows two well-refined anodic peaks at 4.12 and 4.2 V and a corresponding pair of cathodic peaks at 3.89 and 4.02 V. The appearance of such peaks are characteristic of $LiMn_2O_4$-based spinels and analogous to Li^+ extraction and insertion, which in turn reflects the typical Mn^{3+}/Mn^{4+} redox process of the spinel structure in the 4 V domain [21]. The perfect reversibility

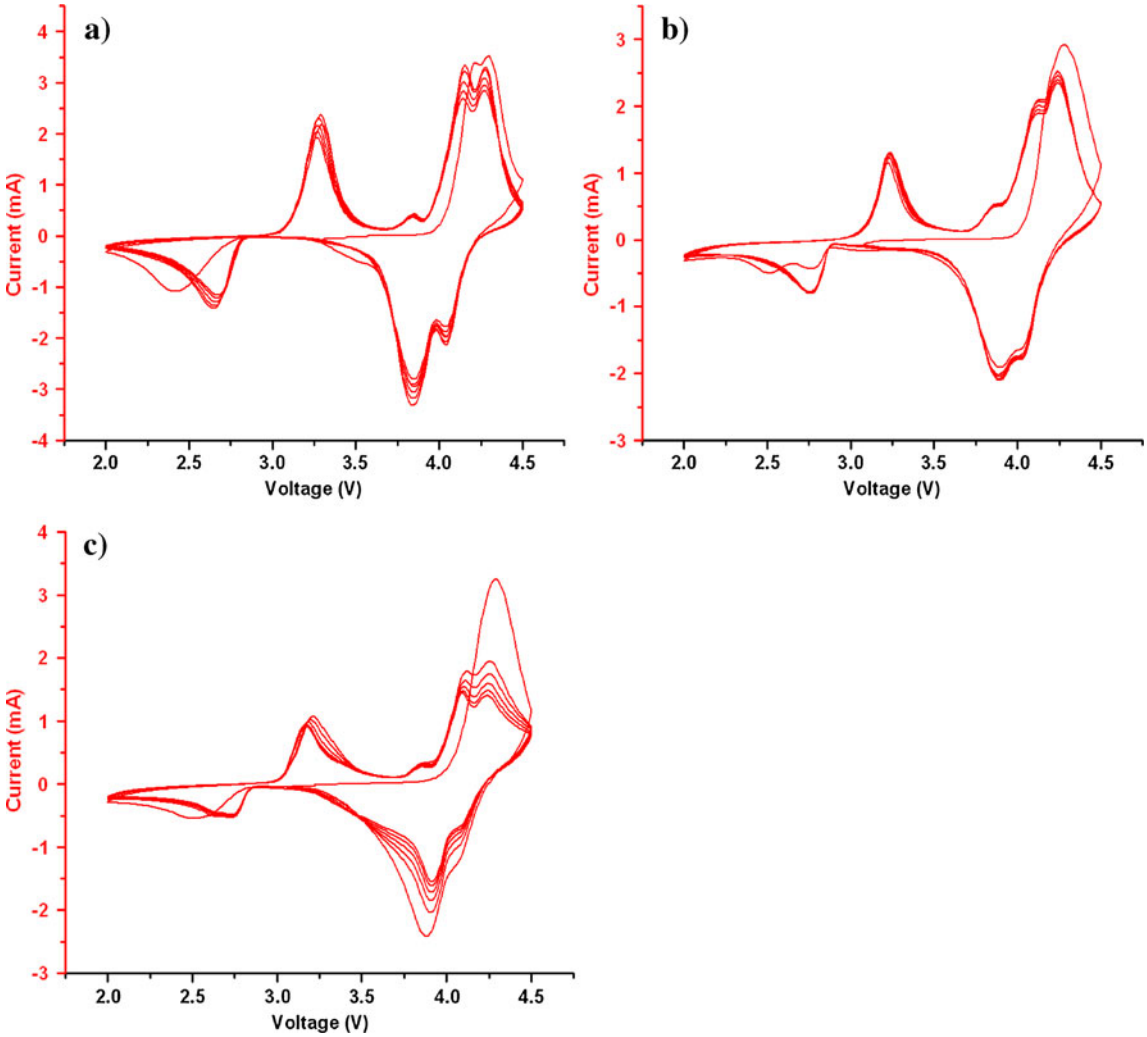

Fig. 5 Cyclic voltammograms of **a** $LiMn_2O_4$, **b** $LiCr_{0.2}Mn_{1.8}O_4$, and **c** $LiV_{0.2}Cr_{0.2}Mn_{1.6}O_4$ recorded at a scan rate of 0.5 mV/s

(overlapping) of the anodic and cathodic peak positions upon progressive cycling of $LiCr_{0.2}Mn_{1.8}O_4$ (Fig. 5b) is an indication that the substitution of Cr^{3+} in to the *16d* octahedral interstices of the spinel matrix has stabilized the cubic spinel structure by excluding the formation of series of cation-ordered phases during charging [4].

On the other hand, the CV pattern of bi-cation substituted $LiCr_{0.2}V_{0.2}Mn_{1.6}O_4$ cathode (Fig. 5c) displayed a poor reversibility accompanied by a significantly reduced peak current. This may be viewed as a result of Mn^{3+}/V^{5+}-induced defect mechanism that probably promotes a fraction of vanadium to occupy *8a* tetrahedral interstices [22], thus responsible for the reduced lithium diffusion kinetics. In addition, the larger difference in the XRD lattice parameter value is expected to cause an instantaneous volume change in the 4 V two-phase region, which is analogous to the Jahn–Teller distortion-driven volume change occurring in 3-V region. Hence, it is understood from the study that the advantageous effect of Cr^{3+} dopant is offset by the V^{5+} dopant, which is unavoidable.

Besides the presence of two pairs of peaks for the 4 V process, there appeared a pair of distinguished peaks at 3.23 V on charge and 2.75 V on discharge as shown in Fig. 5a–c. Such a 3 V-region peak pair corresponds to the intercalation of lithium into $LiMn_2O_4$, and the appearance of an extra peak at 3.85 V (from second charging onwards) is attributed to the deintercalation of residual lithium that occupies the octahedral sites, especially during the initial overdischarge of $LiMn_2O_4$-related spinels to 2 V region [23]. Hence, it is understood that the presence of 3.85 V peak from the second cycle onwards is due to the partial occupation of lithium in octahedral sites which are difficult to be extracted at 3.23 V itself [23]. Therefore, it is clearly understood at this point that the previously discussed vanadium-driven presence of 0 ppm resonance in ^7Li NMR and the reduced CV peak current value exhibited by $LiV_{0.2}Cr_{0.2}Mn_{1.6}O_4$ spinel are due to the residual lithium occupation in *16d* octahedral sites. Further, the presence of cathodic peak at 2.75 V substantiates the fact that the stability of doped spinel cathode is maintained upon over

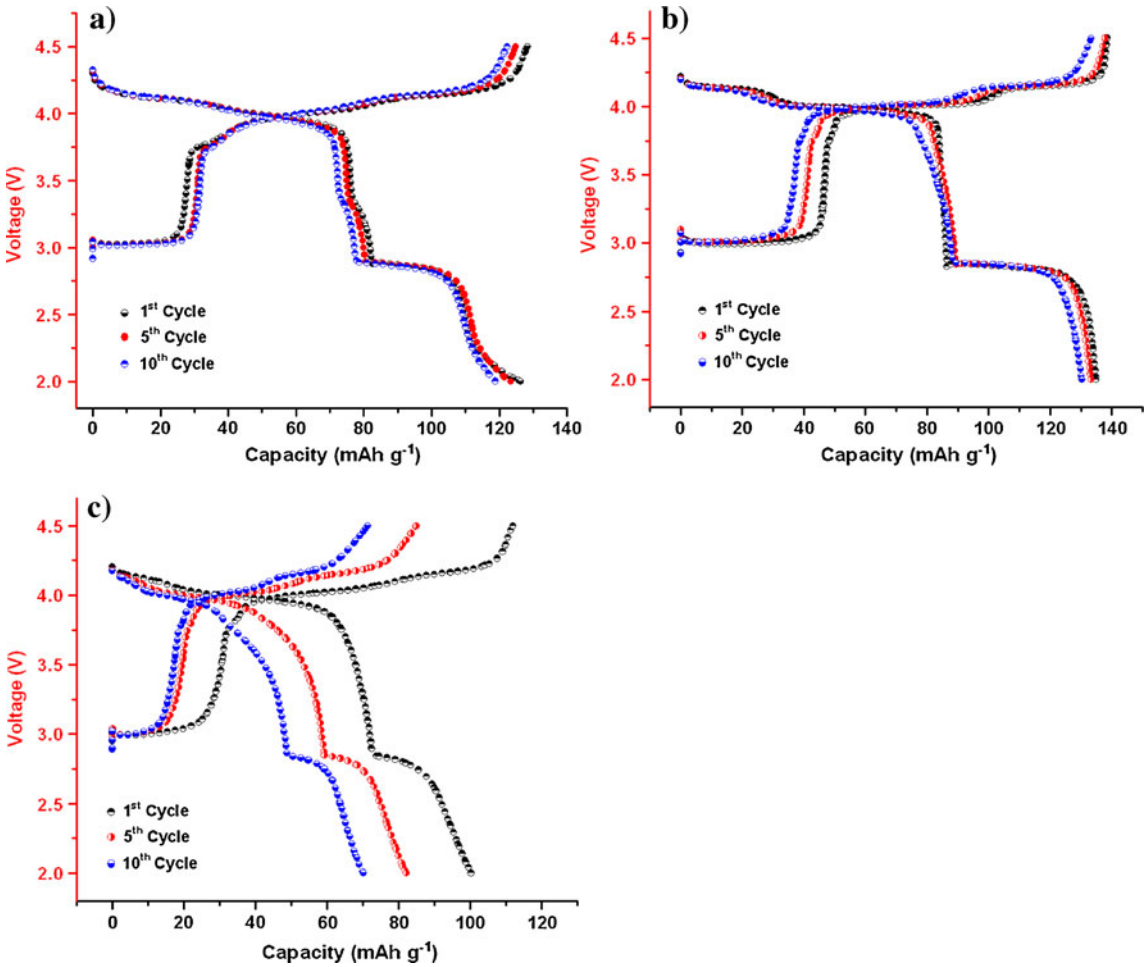

Fig. 6 Voltage vs. capacity behavior of **a** $LiMn_2O_4$, **b** $LiCr_{0.2}Mn_{1.8}O_4$, and **c** $LiV_{0.2}Cr_{0.2}Mn_{1.6}O_4$

discharging of cathodes well below 3 V, which is the highlight of the present study.

Electrochemical charge–discharge studies

Figure 6a–c exhibits the typical charge and discharge profile of $Li/LiMn_2O_4$, $Li/LiCr_{0.2}Mn_{1.8}O_4$, and $Li/LiV_{0.2}Cr_{0.2}Mn_{1.6}O_4$ cells under the influence of 0.2 mA current. When the parent $LiMn_2O_4$ is cycled, the discharge profile displayed typical plateaus at about 4.0, 4.15, 3.3, and 2.8 V, among which the plateaus at 4.0 and 4.15 V are attributed to the insertion and extraction of lithium ions in two stages [24]. Further, the discharge plateau exposed in between 2.7 and 3.0 V (~2.8 V) may be related to the 3 V processes of $LiMn_2O_4$ (Fig. 6a) corresponding to the insertion/extraction of lithium between cubic $LiMn_2O_4$ and tetragonal $Li_2Mn_2O_4$ [25].

It is obvious from Fig. 6b that the Cr-substituted spinel cathode has exhibited nominal two-phase region at the 4 V domain, which is in agreement with the peak intensities of the CV redox pairs observed with $LiCr_{0.2}Mn_{1.8}O_4$ spinel cathode (Fig. 5b). As reported by Sigala et al. [12],

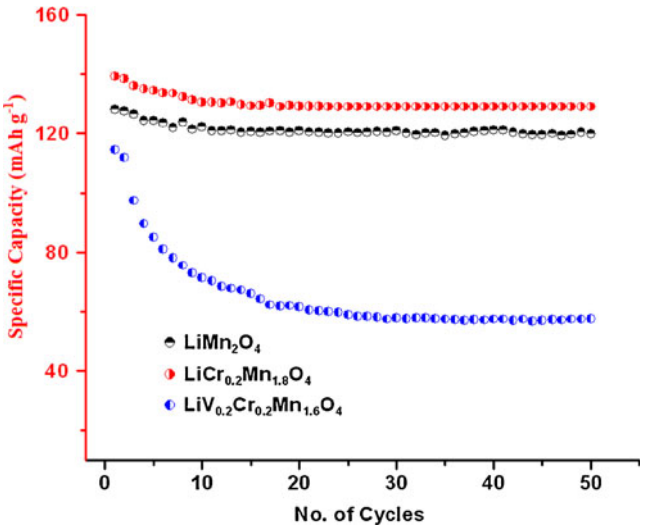

Fig. 7 Specific capacity vs. cycle life behavior corresponding to 2.0 ~ 4.5 V region

appearance of Cr^{3+}/Cr^{4+} redox peak at 4.3 V and the co-existence of Cr^{3+}, Mn^{3+}, and Mn^{4+} at 3.5 V in $LiCr_{0.2}Mn_{1.8}O_4$ could be understood. The discharge plateau at 3.3 V becomes indistinguishable (Fig. 6b) for $LiCr_{0.2}Mn_{1.8}O_4$, and the 4 V region plateau corresponds to a capacity of 85 mAh/g (Fig. 6b) against 78 mAh/g (Fig. 6a) of $LiMn_2O_4$ cathode.

It is reported that with the higher concentration of Cr ($x>0.30$) substitution, an irreversible displacement of Cr^{3+} and Mn^{3+} ions from the *16d* to *8a* positions is possible due to the local oxidation of Cr and Mn to a higher oxidation state of Cr^{6+}, Mn^{6+}, and Mn^{7+} [26]. Such an irreversible T_d occupation of Cr^{3+} will lead to the formation and accumulation of $Cr^{VI}O_4$ groups upon cycling at higher voltages, and due to the presence of few Cr^{6+} in T_d sites, a possible fade in capacity is reported for $LiCr_{0.2}Mn_{1.8}O_4$ spinels with higher concentration of Cr. On the other hand, the currently chosen 10% Cr^{3+} substitution is believed to modify few Mn^{3+} near Cr^{3+} O_h sites to increase the oxidation state of manganese beyond 3.5. Hence, reduced capacity fade and an enhanced structural stability are exhibited by $LiCr_{0.2}Mn_{1.8}O_4$ cathode (Fig. 7). Herein, the excellent capacity retention behavior (94%) of $LiCr_{0.2}Mn_{1.8}O_4$ cathode upon cycling (Fig. 7) results from an increased M-O covalency provided by Cr^{3+} dopant, which is isoelectronic with Mn^{4+}, that prevents the changes in the crystal lattice of the parent $LiMn_2O_4$ [8].

The capacity of the bication-substituted $LiV_{0.2}Cr_{0.2}Mn_{1.6}O_4$ cathode corresponding to 3.5 V cut-off region encountered a decreased capacity value of 70 mAh/g (Fig. 6c) against 78 mAh/g of $LiMn_2O_4$ cathode (Fig. 6a), and the same may be attributed to the vanadium-driven cation mixing that leads to reduced lithium diffusion kinetics. Such a reduced capacity value is not unusual, as it is reported that specific capacities of 85 and 75 mAh/g are reported for $LiMn_2O_4$ and that of $LiV_{\delta}Mn_{2-\delta}O_4$ cathode, respectively [12]. However, the capacity fade per cycle is large (Fig. 7) for $LiCr_{0.2}V_{0.2}Mn_{1.6}O_4$ cathode (0.96% per cycle), which is an indication of Jahn–Teller distortion-based structural instability problem. Generally, Jahn–Teller distortion occurs when the oxidation state of manganese drops below 3.5 during discharge and is known to form $Li_2Mn_2O_4$ which is associated with a large change in cell volume. The same may be understood from a different angle also, i.e., when the added V^{5+} metal ions pervade the T_d sites of lithium ions (as derived from ^{7}Li NMR study) and block the lithium diffusion channels, ultimately a detrimental effect on lithium intercalation behavior is anticipated. As a result, even though lesser Cr^{3+} concentration is helpful in minimizing the capacity loss behavior of native spinel cathode, the pentavalent vanadium-promoted cation mixing is believed to reduce the Mn^{3+} charge into Jahn–Teller region to exhibit a specific capacity of 70 mAh/g from $LiV_{0.2}Cr_{0.2}Mn_{1.6}O_4$ cathode. Hence, the dual occupancy of vanadium ions both in *8a* and *16d* positions is understood from cycling studies also. In short, $LiV_{0.2}Cr_{0.2}Mn_{1.6}O_4$ cathode exhibits an inferior electrochemical performance, solely due to the presence of V^{5+} dopant that offsets the advantages of Cr^{3+} dopant.

Conclusion

The effect of mono- (Cr^{3+}) and bication (Cr^{3+}, V^{5+}) substitution upon $LiMn_2O_4$ spinel matrix has been studied via synthesis and characterization of a set of $LiMn_2O_4$, $LiCr_{0.2}Mn_{1.8}O_4$, and $LiV_{0.2}Cr_{0.2}Mn_{1.6}O_4$ cathodes. Presence of phase-pure and size-reduced products has been confirmed through XRD and SEM results, respectively. ^{7}Li NMR study reveals the possibility of T_d site occupation of vanadium and a fraction of Li ions in a less preferred *16d* octahedral interstice, especially when V^{5+} is incorporated in the spinel matrix. In this regard, the reduced CV peak current values and the inferior charge–discharge characteristics observed for $LiV_{0.2}Cr_{0.2}Mn_{1.6}O_4$ cathode substantiate the probable cation mixing, induced by the pentavalent V dopant. However, $LiCr_{0.2}Mn_{1.8}O_4$ cathode exhibited better electrochemical stability and capacity retention upon progressive cycling. In addition, the selected CAM sol–gel synthesis methodology has significantly improved the capacity retention behavior of undoped $LiMn_2O_4$ (95%) cathode, which is interesting.

Acknowledgements The authors are thankful to the Department of Science and Technology (DST), India for the financial support to carry out this work.

References

1. Thackeray MM, David WIF, Bruce PG, Goodenough JB (1983) Mater Res Bull 18:461–472
2. Lee YJ, Wang F, Grey CP (1998) J Am Chem Soc 120:2601–12613
3. Ramana CV, Massot M, Julien CM (2005) Surf Interface Anal 37:412–416
4. Grey CP, Dupre N (2004) Chem Rev 104:4493–4512
5. Tarascon JM, Armand M (2001) Nature 414:359–367
6. Ohzuku T, Makimura Y (2001) Chem Lett 30:744
7. Nagaura T, Tozawa K (1990) Prog Batteries Sol Cells 9:209
8. Tucker MC, Reimer JA, Cairns EJ (2002) J Electrochem Soc 149: A574–A585
9. Fu YP, Su YH, Lin CH (2004) Solid State Ionics 166:137–146
10. Tucker MC, Kroeck L, Reimer JA, Cairns EJ (2002) J Electrochem Soc 149:A1409–A1413
11. Sigala C, Guyomard D, Verbaere A, Piffard Y, Tournoux M (1995) Solid State Ionics 81:167–170
12. Hu Y, Liu YH (2005) Mater Chem Phys 90:255–261
13. Jayaprakash N, Kalaiselvi N, Periasamy P (2007) Nanotechnology 19:025603–025608
14. Jayaprakash N, Sathiyanarayanan K, Kalaiselvi N (2007) Electrochim Acta 52:2453–2460
15. Kalaiselvi N, Doh CH, Park CW, Moon SI, Yun MS (2004) Electrochem Commun 6:1110–1113

16. Rojas RM, Petrov K, Avdeev G, Amarilla JM, Pascual L, Rojo JM (2007) J Therm Anal Calorim 90:67–72
17. Morgan KR, Collier S, Burns G, Ooi K (1994) J Chem Soc Chem Commun 2:1719–1720
18. Treuil N, Labruge're C, Menetrier M, Portier J, Campet G, Deshayes A, Frison JC, Hwang SJ, Song SW, Choy JH (1999) J Phys Chem B 103:2100–2106
19. Jayaprakash N, Kalaiselvi N, Gangulibabu, Bhuvaneswari (2010) Electrochimica Acta (in press)
20. Takahashi M, Tobishima SI, Takei K, Sakurai Y (2002) Solid State Ionics 148:283–289
21. Striebel KA, Deng CZ, Wen SJ, Cairns EJ (1996) J Electrochem Soc 143:1821–1827
22. Kalyani P, Kalaiselvi N, Renganathan NG (2005) Mater Chem Phys 90:196–202
23. Tang SB, Lai MO, Lu L (2006) Electrochim Acta 52:1161–1168
24. He BL, Zhou WJ, Liang YY, Bao SJ, Li HL (2006) J Colloid Interfac Sci 300:633–639
25. Tang SB, Lai MO, Lu L (2007) J Power Sources 164:372–378
26. Sigala C, Verbaere A, Mansot JL, Guyomard D, Piffard Y, Tournoux M (1997) J Solid State Chem 132:372–381